Article

Journal of
Nanoscience and Nanotechnology
Vol. 16, 10535–10540, 2016
www.aspbs.com/jnn

Improved Methanol Electro-Oxidation of Pt Electrocatalysts on Porous Carbon Nanofiber–Ruthenium Core–Shell Supports

Dong-Yo Sin, Geon-Hyoung An, and Hyo-Jin Ahn*

Department of Materials Science and Engineering, Seoul National University of Science and Technology, Seoul 139-743, South Korea

Well-dispersed Pt electro-catalysts decorated on porous carbon nanofiber–Ru core–shell supports were synthesized using co-electrospinning followed by a reduction method for improved methanol electro-oxidation. To determine the optimum conditions for porous carbon nanofiber–Ru core–shell supports, we prepared three different loading amounts of the Ru shell layer: 10 wt% (sample A), 20 wt% (sample B), and 30 wt% (sample C). Of the three, sample B exhibited the highest methanol electro-oxidation (~741.1 mA/mg$_{Pt}$), excellent poison tolerance, and superb electrocatalytic stability compared with Pt/carbon nanofiber and commercial Pt/C. The enhanced electrochemical performance can be explained by the combined effects of well-dispersed Pt electro-catalysts on porous carbon nanofiber–Ru core–shell supports, an optimum loading of the Ru shell layer on the porous carbon nanofiber surface, and the high surface area of porous carbon nanofiber in the core region.

Keywords: Methanol Electro-Oxidation, Platinum Electro-Catalysts, Porous Carbon Nanofiber–Ruthenium Core–Shell Supports, Co-Electrospinning, A Reduction Method.

1. INTRODUCTION

Direct methanol fuel cells (DMFCs) have received considerable interest as next-generation energy devices to solve the problems of environmental pollution and energy depletion.[1,2] In general, DMFCs are composed of an anode, a cathode, a membrane, and an electrolyte. DMFCs have attractive advantages, including high energy density, high energy-conversion efficiency, eco-friendly operation, and a low operating temperature.[1,2] However, in spite of these advantages, DMFCs possess critical disadvantages, such as the need for expensive Pt electrocatalysts, poor durability due to carbon monoxide poisoning, low electrocatalytic activity, and methanol crossover. Among the above-mentioned disadvantages, the need for expensive Pt electrocatalysts is one of main barriers to the industrial use of DMFCs.[3] Previous researchers have studied many strategies to reduce the amount of Pt electrocatalysts, such as controlling the size, morphology, and crystal plan of the Pt electrocatalysts; alloying them with various metals; and introducing support materials.[4–7] One promising strategy has been to introduce effective catalyst supports such as carbon-based materials (graphite, graphene, carbon nanotubes (CNTs), and carbon nanofibers (CNFs)); metal oxide-based materials (TiO_2, SnO_2, Co_3O_4, indium tin oxide (ITO), and WO); and conducting polymers (poly(diallyldimethylammonium) chloride (PDDA), poly(3,4-ethylenedioxythiophene) (PEDOT), and poly(N-acteylaniline)).[8,9] In particular, carbon-based materials as supports for improving the electrocatalytic activity have attracted intense interest on the part of many researchers because of their unique structure, physical/chemical stability, low-cost, excellent electrical conductivity, and large surface areas.[10] CNFs are of considerable interest because of their advantages such as high specific surface area (448 m^2/g), low electrical resistivity (1.7×10^3), and thermal and chemical stability, as well as their one-dimensional nanostructure that gives rise to an efficient electron transport.[11] For example, Sebastian et al. synthesized Pt catalyst-loaded CNFs using a reduction method; the current density (1.71 mA/cm^2) of their Pt catalyst-loaded CNFs for methanol electro-oxidation was higher than that of commercial Pt/C (Vulcan XC-72R

*Author to whom correspondence should be addressed.

carbon black) (0.66 mA/cm^2).[12] Hsin et al. fabricated PtRu particle-loaded CNFs using chemical vapor deposition; the current density (104.6 mA/mg$_{Pt}$) of these PtRu particle-loaded CNFs was greater than that of the commercial Pt/C (Vulcan XC-72R carbon black) (35.2 mA/mg$_{Pt}$).[13] Zhao et al. fabricated Pt particle-loaded porous CNFs (PCNFs) using a self-assembly method; they reported a current density (69.6 mA/cm^2) for methanol electro-oxidation that was higher than that of the commercial Pt/C (E-TEK) (40.3 mA/cm^2).[14] Nevertheless, research on the introduction of PCNF–Ru core–shell supports for improved methanol electro-oxidation has not yet been reported. In addition, we selected the Ru materials due to their excellent CO-tolerance during the methanol electro-oxidation. The excellent CO-tolerance on catalysts can provide the improved electrocatalytic activity using bifunctional effect ($Ru–OH + Pt–CO \rightarrow Pt + Ru + CO_2 + H^+ + e^-$). The existence of Ru could assist the Pt–CO_{ads} oxidation at low potential by the abundant adsorbed hydroxyl (Ru–OH_{ads}) species.[15, 16]

In the present study, we synthesized well-dispersed Pt electrocatalysts decorated on PCNF–Ru core–shell supports using co-electrospinning and a reduction method, and demonstrated their improved methanol electro-oxidation for use as anode in DMFCs.

2. EXPERIMENTAL DETAILS

In order to synthesize the PCNF, two types of solutions for co-electrospinning were prepared as follows: For the core region, a mixed solution of 8 wt% tin (‖) chloride dihydrate ($SnCl_2 \cdot 2H_2O$, ≥99.995%, Aldrich) and poly(vinylpyrrolidone) (PVP, M_w = 1,300,000 g/mol, Aldrich) was dissolved in *N*,*N*-Dimethylformamide (DMF, 99.8%, Aldrich). For the shell region, a mixed solution of polyacrylonitrile (PAN, M_w = 150,000, Aldrich) and PVP was dissolved in DMF. For the co-electrospinning process, the feeding rates into the core region and the shell region were set at 0.02 mL/h and 0.04 mL/h, respectively, and the distance between the collector and the syringe needle was fixed at ∼15 cm. The voltage and humidity were maintained at ∼17 kV and 10% during co-electrospinning. The as-spun nanofibers were stabilized at 280 °C for 2 h in an air atmosphere and then carbonized at 800 °C for 2 h in a N_2 atmosphere, resulting in CNFs with embedded SnO_2 nanoparticles. In order to obtain PCNF, the CNFs with the embedded SnO_2 nanoparticles were reduced using the gas mixture (H_2:N_2 = 1:9 v/v) at 800 °C for 20 h. Sn nanoparticles were agglomerated on the CNF surface by a H_2-reduction method, then the Sn nanoparticles were removed by an acid treatment using a mixture of hydrogen fluoride (HF, 52%) and nitric acid (HNO_3, 66%). In this manner, the PCNF supports were synthesized successfully. In order to synthesize PCNF–Ru core–shell supports, the PCNF was dispersed in DI-water. To obtain 10 wt%, 20 wt%, and 30 wt% Ru shell layers, we prepared solutions of $RuCl_3 \cdot xH_2O$ (Aldrich) at three different concentrations: 0.28, 0.56, and 0.84 mM; these were then added to the PCNF-dispersed solutions. $NaBH_4$ solution was used as a reducing agent for the formation of the Ru shell layer on the PCNF surfaces, which were then dried at 80 °C in a drying oven. Finally, to synthesize well-dispersed Pt electrocatalysts on the PCNF–Ru core–shell supports, the supports were decorated with 20 wt% Pt using a reduction method with $H_2PtCl_6 \cdot xH_2O$ (Aldrich). Specifically, the PCNF–Ru core–shell supports were dispersed in DI-water and then $H_2PtCl_6 \cdot xH_2O$ was added to the dispersion solution at a concentration of 0.56 mM. Next, concentrated $NaBH_4$ solution was added. After being washed several times, the resultant samples were freeze-dried at −50 °C using liquid nitrogen. Commercial Pt/C catalysts (20 wt% Pt on Vulcan carbon, E-TEK, now a division of Industrie De Nora S.P.A., Italy) were prepared for comparison purposes. In addition, 20 wt% Pt electrocatalysts on PCNF supports without the Ru shell layer were prepared by the above-mentioned method. Thus, we obtained 20 wt% Pt electrocatalysts on PCNF supports, PCNF–10 wt% Ru core–shell supports, PCNF–20 wt% Ru core–shell supports, and PCNF–30 wt% Ru core–shell supports (referred to herein as Pt/PCNF, sample A, sample B, and sample C, respectively).

The structural and morphological properties of the samples were determined by field emission-scanning electron microscopy (FESEM; Hitachi S-4800) and transmission electron microscopy (TEM; JEOL 2100F, KBSI Suncheon Center). The crystal structures and chemical bonding states were examined by X-ray diffractometry (XRD, Rigaku D/MAX2500 V) and X-ray Photoelectron spectroscopy (XPS, ESCALAB 250 equipped with an Al K_α X-ray source), respectively. Electrochemical performance measurements were carried out with a potentiostat/galvanostat (PGST302N by Eco Chemie, Netherlands) using a conventional three-electrode system consisting of a working electrode (a glassy carbon electrode with an area of 0.07 cm^2), a counter electrode (Pt gauze), and a reference electrode (Ag/AgCl, saturated KCl). The electrolyte was a mixture of 0.5 M H_2SO_4 and 2 M CH_3OH. To measure methanol electro-oxidation, all samples were prepared as mixed inks of 80 wt% electrocatalysts and 20 wt% Nafion (Aldrich). Inks of all samples were coated on glassy carbon electrodes. The electrocatalytic activity for methanol electro-oxidation was evaluated by cyclic voltammetry (CV) at a scan rate of 50 mV/s in the range of −0.2 to 1.0 V. The electrocatalytic stability was examined by chronoamperometry (CA) in a mixture of 0.5 M H_2SO_4 and 2 M CH_3OH at a constant voltage of 0.5 V for 2000 s.

3. RESULTS AND DISCUSSION

Figure 1 shows a schematic illustration of the synthesis steps for well-dispersed Pt electrocatalysts on PCNF–Ru core–shell supports using co-electrospinning followed by

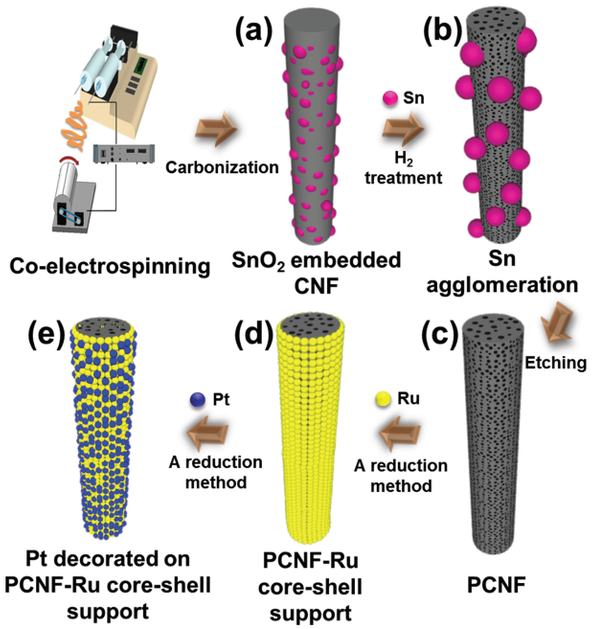

Figure 1. Schematic illustration of the synthesis steps for well-dispersed Pt electrocatalysts on PCNF–Ru core–shell supports.

a reduction method. First, SnO_2-embedded CNFs were synthesized by co-electrospinning (Fig. 1(a)). Next, Sn nanoparticles were aggregated on the CNF surface using a reduction reaction by H_2-treatment (Fig. 1(b)). The agglomerated Sn particles were then removed by acid treatment (Fig. 1(c)). To obtain well-dispersed Pt electrocatalysts on the supports, the 20 wt% Ru shell layers were uniformly loaded by a reduction method (Fig. 1(d)). Finally, well-dispersed Pt electrocatalysts were successfully synthesized on PCNF–Ru core–shell supports by a reduction method (Fig. 1(e)).

Figure 2 shows FESEM images obtained from PCNF, Pt/PCNF, sample A, sample B, and sample C. The diameters of the samples were in the range of ∼142.60 to ∼158.79 nm for PCNF, ∼154.43 to ∼168.43 nm for Pt/PCNF, ∼142.59 to ∼165.54 nm for sample A, ∼142.02 to ∼158.28 nm for sample B, and ∼142.84 to ∼159.92 nm for sample C. The PCNF (Fig. 2(a)) had a rough CNF surface, which is in good agreement with previously reported works.[11] Also, the PCNFs had a high specific surface area of 1053 m^2/g compared to the conventional CNFs (433 m^2/g) that use only PAN in the electrospinning solution; the difference is due to the removal of the Sn particles. The Pt/PCNF (Fig. 2(b)) showed significant agglomeration of the Pt electrocatalysts because of strong carbon−carbon bonding at the CNF surface.[9] In order to overcome this problem, PCNF–Ru core–shell supports were employed in this work with the optimum loading amount of the Ru shell layer on the CNF surface. Samples A–C exhibited improved dispersion of the Pt electrocatalysts on the supports, compared to the Pt/PCNF, because of the existence of the Ru shell layer. Among three cases, sample B exhibited the smoothest PCNF surface without agglomeration of Pt electrocatalysts; this indicates good dispersion of the Pt electrocatalysts on the supports. Furthermore, sample C (Fig. 2(e)) showed a highly agglomerated PCNF surface because of the high loading amount (30 wt%) of the Ru shell layer on the PCNF surface, which constrains the uniform dispersion of the Pt electrocatalysts. In methanol electro-oxidation, the agglomeration of Pt electrocatalysts on the PCNF surface could result in a severe reduction of electrocatalytic activity.

To further investigate the morphological and structural properties of the samples, TEM measurements were carried out, as shown in Figure 3, which presents TEM images obtained from Pt/PCNF, sample A, sample B, and sample C. Pt/PCNF (Fig. 3(a)) showed large agglomerated Pt electrocatalysts (see dark contrast) on the PCNF supports. Sample A (Fig. 3(b)) shows agglomerated Pt electrocatalysts on the supports owing to the low loading amount (10 wt%) of the Ru shell layer on the PCNF surface. Thus, the low loading amount (10 wt%) of the Ru shell layer could not perfectly wrap on the CNF surface (Fig. 3(b)), resulting in the agglomeration of Pt electrocatalysts due to the strong carbon–carbon bonds at the CNF surface.[3] Among samples A–C, sample B (Fig. 3(c)) demonstrated the best dispersion of Pt electrocatalysts on the PCNF–Ru core–shell supports with clusters 3–6 nm in size. On the other hand, sample C (Fig. 3(d)) exhibited highly agglomerated Pt elctrocatalysts on the supports as a result of the high loading amount (30 wt%) of the Ru shell layer on the PCNF surface. Therefore, the high loading amount (30 wt%) of the Ru shell layer could incur the agglomerated Ru shell layer, resulting in the agglomeration of Pt electrocatalysts after a reduction method. Therefore, sample B showed the best dispersion of the Pt electrocatalysts decorated on the PCNF–Ru core–shell supports. To demonstrate the good distribution of Pt and Ru atoms for sample B, TEM–energy dispersive spectroscopy (TEM–EDS) mapping analysis was performed, as shown in Figure 3(e). Pt and Ru atoms were uniformly dispersed on the PCNF, and Pt atoms were widely dispersed on the PCNF–Ru core–shell supports. Based on SEM, TEM, and TEM–EDS mapping results, it can be concluded that the introduction of a Ru shell layer on the PCNF surface can directly affect the formation of well-dispersed Pt electrocatalysts because the crystal structure of Ru is similar to the hexagonal structure of CNF.[3] In addition, the optimum loading amount of the Ru shell layer on the PCNF is 20 wt%.

Figure 4(a) shows XRD data for PCNF, Pt/PCNF, sample A, sample B, and sample C. The PCNFs indicated broad peaks at around 25°, corresponding to the (002) layers of graphite. The main peaks of Pt/PCNF, sample A, sample B, and sample C were observed at $2\theta = 39.7°$, 46.2°, 67.4°, and 81.3°, respectively. These peaks correspond to the (111), (200), (220), and (311) planes of a face-centered cubic structure of Pt phases of the space

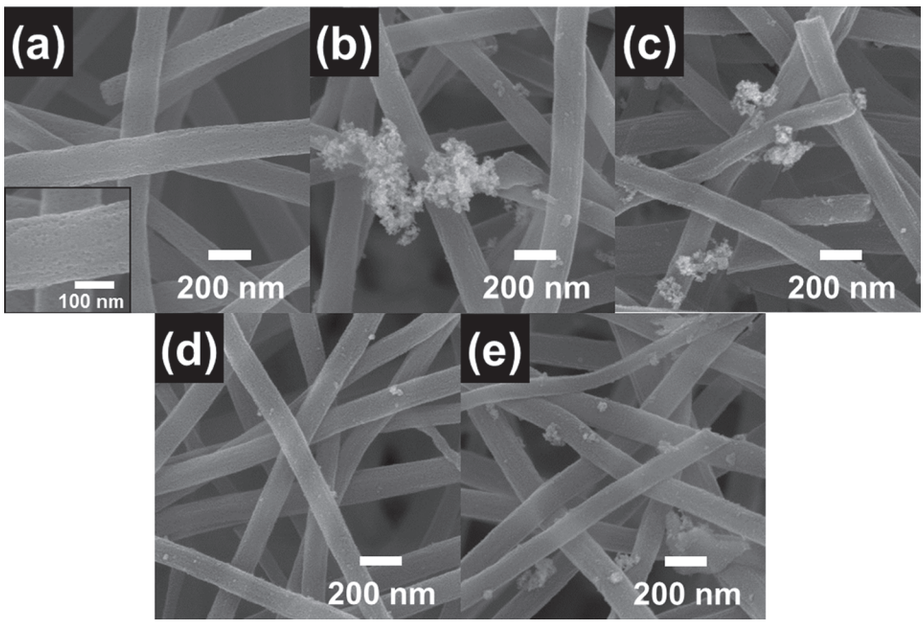

Figure 2. FESEM images obtained from (a) PCNF, (b) Pt/PCNF, (c) sample A, (d) sample B, and (e) sample C.

group *Fm3m*[225] (JCPDS card No. 04-0802). Additional peaks caused by the PCNF–Ru core–shell supports were observed at 38.4°, 42.1°, and 44.0°, corresponding to the (100), (002), and (101) planes of the hexagonal structure of Ru phases of the space group $P6_3/mmc$[194] (JCPDS card No. 06-0663). Also, the peak shift of Ru did not occur at high angles because we are not observing PtRu alloy, but rather, independent Pt and Ru phases. In addition, samples A–C were observed to have broad peaks around 37°–45° because the peak intensity of the (101) plane of Ru increased with increasing loading amount of the Ru shell layer. Figures 4(b and c) show XPS spectra of Pt $4f$ and Ru $3p$ core levels for sample B. The XPS core-level spectra from Pt $4f_{7/2}$ and Pt $4f_{5/2}$ photoelectrons were observed at ~71.3 eV and ~74.4 eV, respectively, indicating the metallic Pt phases.[17] The Ru $3p$ XPS spectral peaks showed two different signals at ~462.6 eV and ~485.0 eV, corresponding to the Ru $3p_{3/2}$ and Ru $3p_{1/2}$ photoelectrons, respectively, of the metallic Ru phases as previously reported.[18] Based on the SEM, TEM, TEM–EDS mapping, XRD, and XPS results, it can be seen that well-dispersed Pt electrocatalysts on PCNF–Ru core–shell supports were successfully synthesized.

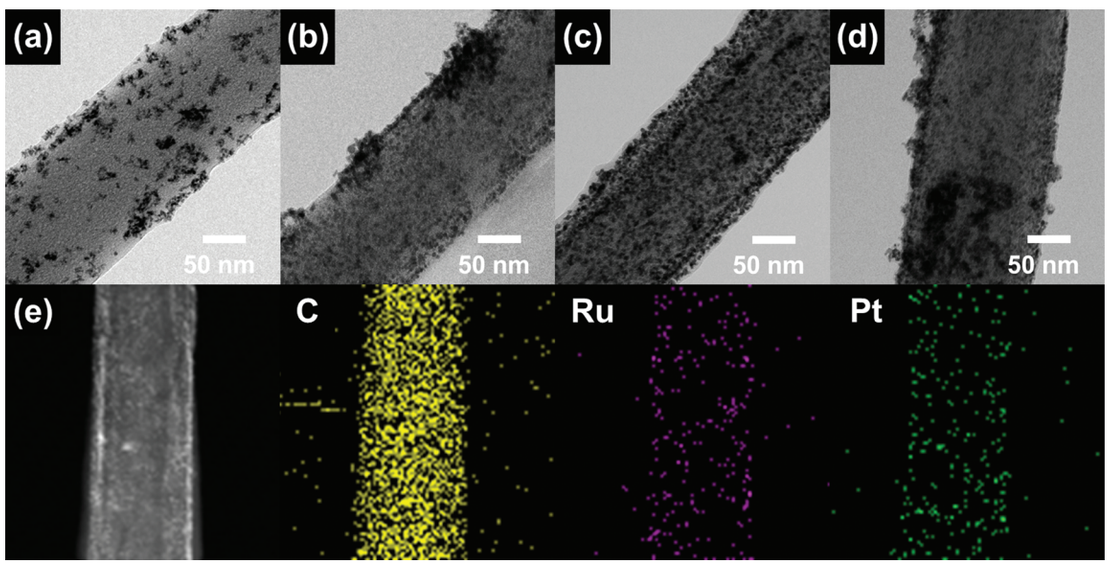

Figure 3. TEM images of (a) Pt/PCNF, (b) sample A, (c) sample B, and (d) sample C. (e) TEM–EDS mapping data of sample B.

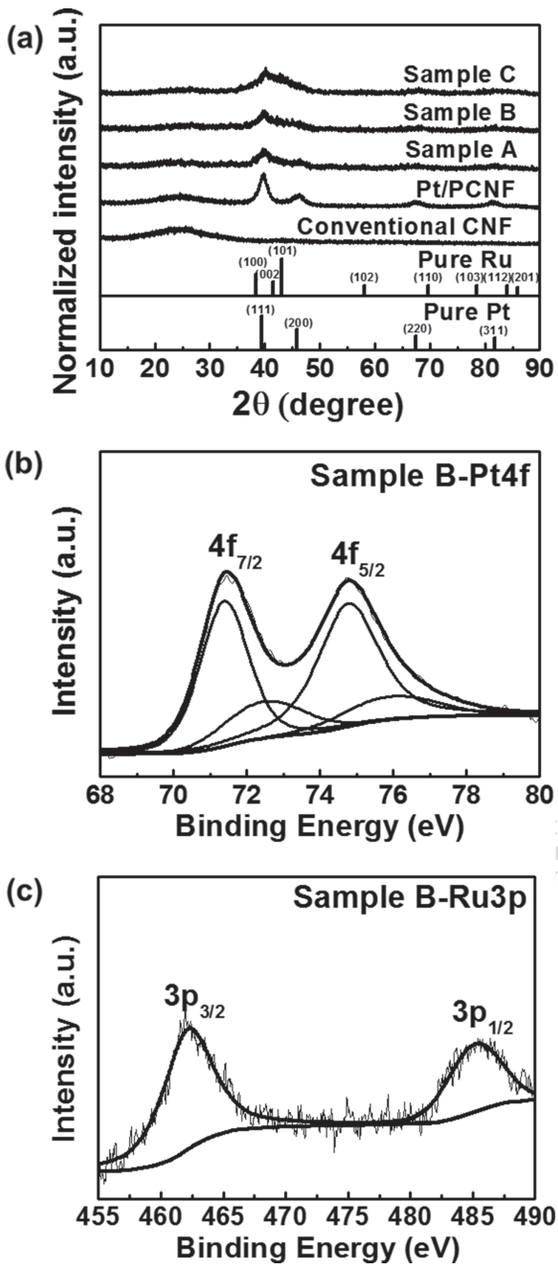

Figure 4. (a) XRD data of PCNF, Pt/PCNF, sample A, sample B, and sample C. (b) XPS spectra of Pt 4f and Ru 3p core levels of sample B.

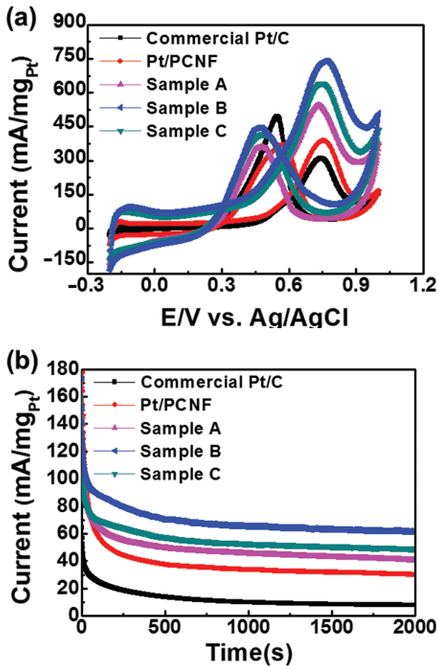

Figure 5. (a) Cyclic voltammetry curves of methanol electro-oxidation of commercial Pt/C, Pt/PCNF, samples A, sample B, and sample C. (b) Chronoamperometry of commercial Pt/C, Pt/PCNF, samples A, sample B, and sample C in a solution of 0.5 M H_2SO_4 and 2 M CH_3OH at 0.5 V.

Figure 5(a) shows the cyclic voltammetry (CV) curves of methanol electro-oxidation for all the samples. Commercial Pt/C catalysts (20 wt% Pt on Vulcan carbon, E–TEK) were prepared for comparison. The CV curves displayed two peaks designated as forward and backward peaks. A forward peak implies anodic current density, whereas a backward peak implies intermediate species such as CH_2OH, CHO, HCOOH, and CO.[19] In general, methanol electro-oxidation at the anode generates carbon dioxide, 6 protons, and 6 electrons according to the following formula:[20]

$$CH_3OH + H_2O \rightarrow 6e^- + 6H^+ + CO_2 \quad (1)$$

The higher forward peak (I_f) corresponds to the number of electrons produced at the anode. The anodic current densities of the commercial Pt/C, Pt/PCNF, sample A, sample B, and sample C are ~291.4, ~388.0, ~481.11, ~741.1, and ~543.0 mA/mg_{Pt}, respectively. The anodic current density is directly related to electrocatalytic activity for methanol electro-oxidation. Thus, sample B exhibited the best electrocatalytic activity for methanol electro-oxidation among all the samples owing to the well-dispersed Pt electrocatalysts on the PCNF–Ru core–shell supports. However, sample C showed a lower current density than sample B because of agglomeration of the Ru shell layer on the PCNF, as shown in Figure 3(d). Moreover, the backward anodic peak (I_b) indicates the formation of intermediate species (CH_2OH, CH_2O, HCOOH, and CO) during the forward anodic scan. Thus, the high I_f/I_b ratio indicates the excellent poison tolerance of the electrocatalysts. The I_f/I_b ratios of the commercial Pt/C, Pt/PCNF, sample A, sample B, and sample C were 0.63, 1.05, 1.57, 1.67, and 1.54, respectively. In other words, the I_f/I_b ratio of sample B was the highest of all the samples, implying that the poison tolerance of sample B is excellent during the methanol electro-oxidation. This can be explained by the existence of optimum amount of the Ru

shell layer on PCNF, resulting in the superb bifunctional mechanism.[21] Figure 5(b) shows the CA curves of all samples; these curves can be used to investigate the electrocatalytic stability. All samples incur a current decay during the initial stage owing to the formation of interfering species such as CHO_{ads} and CH_3OH_{ads}, and the adsorption of SO_4^{2-} on the Pt surface. Interfering species and adsorption of SO_4^{2-} would decrease the electrocatalytic reaction area between the electrolyte and the Pt electrocatalysts.[22] Nevertheless, among all the samples, sample B exhibited the best slow-current decay measured during 2000 s, which means that sample B shows superior electrocatalytic stability. Thus, the performance improvement can be explained by three main effects. First, well-dispersed Pt electrocatalysts on the PCNF–Ru core–shell supports with the optimum condition (20 wt%) of the Ru shell layer can achieve increased electrocatalytic activity and stability owing to increased reaction area between the Pt electrocatalysts and the electrolyte. Second, the optimum amount (20 wt%) of the Ru shell layer provide excellent poison tolerance using the bifunctional effect. Finally, the high surface area of PCNF in the core region can assist by increasing loading amount of the Ru shell layer. Therefore, these results imply that PCNF–Ru core–shell supports could be used as promising supports for highly efficient DMFCs.

4. CONCLUSION

Well-dispersed Pt electrocatalysts on PCNF–Ru core–shell supports were successfully synthesized using co-electrospinning, a H_2-treatment, an acid treatment, and a reduction method. To study well-dispersed Pt electrocatalysts on supports, we prepared three loading amounts with 10 wt% (sample A), 20 wt% (sample B), and 30 wt% (sample C) of the Ru shell layer. Of the three, sample B showed the highest anodic current densities of ~741.1 mA/mg_{Pt}, superb poison tolerance, and excellent electrocatalytic stability when compared to all the other samples. The improved electrochemical performance can be attributed to three main causes: (a) effects of the well-dispersed Pt electrocatalysts on PCNF–Ru core–shell supports, (b) an optimized amount (20 wt%) of the Ru shell layer, and (c) the formation of PCNF having a high specific surface area in the core region.

Acknowledgments: This work was supported by the International Collaborative Energy Technology R&D Program of the Korea Institute of Energy Technology Evaluation and Planning (KETEP), granted financial resource from the Ministry of Trade, Industry and Energy, Republic of Korea. (No. 2138520030800).

References and Notes

1. Z. Yin, Y. Zhang, K. Chen, J. Li, W. Li, P. Tang, H. Zhao, Q. Zhu, X. Bao, and D. Ma, *Sci. Rep.* 4, 4288 (**2014**).
2. Y. Li, W. Gao, L. Ci, C. Wang, and P. M. Ajayan, *Carbon* 48, 1124 (**2010**).
3. G.-H. An and H.-J. Ahn, *J. Electroanal. Chem.* 707, 74 (**2013**).
4. K. Yamamoto, T. Imaoka, W. J. Chun, O. Enoki, H. Katoh, M. Takenaga, and A. Sonoi, *Nat. Chem.* 1, 397 (**2009**).
5. G. Zhang, S. Sun, M. Cai, Y. Zhang, R. Li, and X. Sun, *Sci. Rep.* 3, 1526 (**2013**).
6. V. R. Stamenkovic, B. Fowler, B. S. Mun, G. Wang, P. N. Ross, C. A. Lucas, and N. M. Markovic, *Science* 315, 493 (**2007**).
7. Y.-N. Wu, S.-J. Liao, Z.-X. Liang, L.-J. Yang, and R.-F. Wang, *J. Power Sources* 194, 805 (**2009**).
8. H. L. An, G.-H. An, and H.-J. Ahn, *J. Alloys Compd.* 645, 317 (**2015**).
9. Y.-J. Lee, G.-H. Ahn, and H.-J. Ahn, *J. Nanosci. Nanotechnol.* 15, 1 (**2015**).
10. G.-H. An and H.-J. Ahn, *Electrochem. Solid-State Lett.* 3, M29 (**2014**).
11. G.-H. An and H.-J. Ahn, *Carbon* 65, 87 (**2013**).
12. N. Tsiouvaras, M. V. Martinez-Huerta, R. Moliner, M. J. Lazaro, J. L. Rodriguez, E. pastor, M. A. Pena, and J. L. G. Fierro, *J. Power. Sources* 186, 299 (**2009**).
13. Y. L. Hsin, K. C. Hwang, and C.-T. Yeh, *J. Am. Chem. Soc.* 129, 9999 (**2007**).
14. G. Zhao, J. He, C. Zhang, J. Zhon, X. Chen, and T. Wang, *J. Phys. Chem. C* 112, 1028 (**2008**).
15. J. R. C. Salgado, F. Alcaide, G. Alvarez, L. Calvillo, M. J. Lazaro, and E. Pastor, *J. Power. Sources* 195, 4022 (**2010**).
16. J. Guo, G. sun, Q. Wang, G. Wang, Z. Zhou, S. Tang, L. Jiang, B. Zhou, and Q. Xin, *Carbon* 44, 152 (**2006**).
17. J. F. Moulder, W. F. Stickle, P. E. Sobol, and K. D. Bomben, Handbook of X-ray Photoelectron Spectroscopy, Physical Electronics, Eden Pairie, MN, U.S.A (**1995**), pp. 180–181.
18. C. Bock, C. Paquet, M. Couillard, G. A. Botton, and B. R. Macdougall, *J. Am. Chem. Soc.* 126, 8028 (**2004**).
19. Y. Gu, J. Luo, Y. Liu, H. Yang, R. Ouyang, and Y. Miao, *J. Nanosci. Nanotechnol.* 15, 3743 (**2015**).
20. J. Prabhuram, T. S. Zhao, and H. Yang, *J. Electroanal. Chem.*, 578, 105 (**2005**).
21. C. Roth, A. J. Papworth, I. Hussain, R. J. Nichols, and D. J. Schiffrin, *J. Electroanal. Chem.* 581, 79 (**2005**).
22. Z. Ji, X. Shen, G. Zhu, K. Chen, G. Fu, and L. Tong, *J. Electroanal. Chem.* 682, 95 (**2012**).

Received: 3 August 2015. Accepted: 8 March 2016.